Consequences of interfacial Fe-O bonding and disorder in epitaxial Fe/MgO/Fe(001) magnetic tunnel junctions

F. Bonell,[1] S. Andrieu,[1] A. M. Bataille,[2] C. Tiusan,[1] and G. Lengaigne[1]
[1]*Institut Jean Lamour, 54506 Vandoeuvre-lès-Nancy, France*
[2]*IRAMIS/LLB, CEA/Saclay, 91191 Gif-Sur-Yvette, France*

(Received 19 December 2008; revised manuscript received 20 February 2009; published 5 June 2009)

We report on a thorough experimental investigation of the influence of an FeO layer at the Fe/MgO interface on the magnetotransport properties in epitaxial Fe/MgO/Fe(001) magnetic tunnel junctions. Interfacial oxygen is introduced by adsorbing O_2 on the bottom Fe(001) layer. The morphology and composition of the FeO film are investigated by means of scanning tunneling microscopy, reflection high-energy electron diffraction, and x-ray photoelectrons spectroscopy. We show that the amount of interfacial oxygen can be precisely tuned and that either ordered or disordered FeO layers can be grown. Both Fe-O bonding and interfacial disorder strongly alter the conductances of junctions. However, the tunnel magnetoresistance remains large (>85%) even for large oxygen exposure. Interfacial Fe-O bonds are found to lower the parallel conductance in agreement with theoretical predictions.

DOI: 10.1103/PhysRevB.79.224405 PACS number(s): 75.70.Cn, 72.25.Mk, 73.40.Gk, 73.40.Rw

I. INTRODUCTION

Magnetic tunnel junctions (MTJs) are of great interest for novel spintronics devices and magnetic sensors. The recent use of MgO as the insulating barrier led to enhanced magnetotransport performances compared to AlO_x-based MTJs, namely, a lower resistance-area product and a higher tunnel magnetoresistance (TMR). The latter is defined as the asymmetry of resistance when the electrodes' magnetizations are parallel (P) or antiparallel (AP): $\mathrm{TMR}=(R_{AP}-R_P)/R_P$. Continuous progress in this field makes nowadays sputtered MgO-based MTJs serious candidates for technological developments.[1]

These major advances are due to a deeper knowledge of the mechanisms which govern spin-polarized tunneling, in particular, in the Fe(001)/MgO(001)/Fe(001) model system. First-principle calculations originally demonstrated the huge potential of this simple stacking and predicted a huge TMR (>1000% at 0 K) arising from the conservation and filtering of wave-function electronic symmetries during a ballistic tunneling process, in addition to the spin conservation.[2,3] These theoretical predictions have been rapidly experimentally demonstrated in high-quality single-crystal Fe/MgO/Fe(001) MTJ systems grown by molecular-beam epitaxy (MBE) (Refs. 4–6) as well as in (001) textured CoFeB/MgO/CoFeB grown by sputtering. The highest TMR ratios were reported in the latter (600% at room temperature).[7]

The simple Fe/MgO/Fe(001) stacking still benefits from most theoretical studies. However, within the complex spin-polarized tunneling physics in single-crystal MTJ devices some points still remain unclear. In particular, after gradual improvements due to progress in the preparation, the TMR of Fe/MgO/Fe(001) MTJs seems to have reached its optimal value, i.e., 250% at 20 K and 180% at room temperature (RT), as reported by several groups.[6,8,9] Consequently, important experimental and theoretical efforts are aimed at understanding this limitation. Real MTJs actually deviate from ideal ones considered in theoretical models: the structural defects are suspected to reduce the filtering efficiency and therefore the magnetoresistive response. This reduction was readily ascribed to the presence of an FeO_x layer at the Fe/MgO interface.[10–12] However, this interfacial oxidation remains controversial since several groups showed no evidence of it.[9,13–15] Moreover *ab initio* calculations predict a very weak interaction between Fe(001) and MgO(001).[16] Therefore, it seems that the presence of FeO at the interface is not specific to the Fe/MgO system but rather depends on the sample preparation. This conclusion is furthermore supported by a theoretical investigation of the MgO growth on Fe(001).[17] However, the structural/chemical characterization of the interface and the magnetotransport measurements are usually not performed on the same samples, which unfortunately makes their correlation difficult to analyze. The only relevant conclusion ruled out up to now was that MTJs exhibiting state-of-the-art TMR ratios do not present any interfacial oxidation.[9,13]

The importance of the question about a possible interfacial FeO layer is related to the high sensitivity of spin-polarized tunneling to interfacial bonding. Calculations predict that even less than 1 monolayer (ML) of interfacial oxygen would drastically alter the TMR and the bias dependence of the conductances.[11,18–20] In a same way, it has been experimentally shown that interfacial carbon also affects the tunneling process.[8] Interestingly, the TMR remains large in this last case and several important characteristics for potential device integration are indeed improved. C-doped MTJs show in particular a higher output voltage,[21] an extremely small $1/f$ noise and a large stability in electric fields.[22] This illustrates the possibility of skillfully tuning the electronic properties of interfaces in Fe/MgO/Fe(001) MTJs by inserting small amounts of an interfacial species.

Some theoretical attempts for modeling real MTJs take into account the effects of disorder.[23–25] Lattice distortions in the barrier and at the interfaces are mostly investigated as well as atomic vacancies in MgO. Defects in the barrier are generally found to lower the junction resistance by favoring hopping or scattering events. The roughness is generally modeled by interfacial disorder. In epitaxial Fe/MgO/Fe(001)

calculations show that introducing a weak and uniform interfacial distortion does not affect the TMR very much. On the contrary, large distortions, which better account for small scale disorder (dislocations, steps, and defects), are expected to strongly alter the TMR.

Up to now, the effects of interfacial oxidation and disorder on the magnetotransport in Fe/MgO/Fe(001) have not been much investigated experimentally.[26] For this purpose, we report here a thorough study of epitaxial MTJs with a controlled oxygen interfacial layer. This oxidized interface is obtained by controlling the adsorption of O_2 on top of the bottom Fe(001) electrode prior to the barrier deposition. The adsorption of oxygen on Fe(001) has been widely studied in the past.[27–35] It was shown that an order/disorder transition can be induced by annealing the oxygen overlayer, leading to a $p(1\times1)$-O 1 ML film on the Fe(001) surface.[29,34,36] This surface allows studying the effect of Fe-O chemical bonds at the interface in a well-ordered MTJ with conservation of the crystalline periodicity at the interface. In contrast, as-deposited oxygen forms a quite disordered layer with a strongly changing morphology within the early stages of adsorption. This makes difficult its characterization, leading to contradictory interpretations reported in the literature. In particular, the absolute oxygen coverage corresponding to the different adsorption stages as well as the large scale morphology of the surface remain unclear.

The present paper is divided in two parts. The first one concerns the preparation of the samples and the *in situ* characterization of oxygen covered Fe(001) surfaces. A structural analysis by means of reflection high-energy electron diffraction (RHEED) and scanning tunneling microscopy (STM) is coupled with a chemical analysis allowed by *in situ* x-ray photoelectrons spectroscopy (XPS). The second part is devoted to magnetotransport in MTJs with O-doped Fe/MgO interfaces. The thorough characterization of oxidized Fe(001) surfaces presented in the first part allows us to partially disentangle the effects of Fe-O bonding and the effects induced by interfacial disorder. The features induced by the interfacial oxygen on the dynamic conductances are also discussed. Concerning the Fe-O bonds, a good agreement is found with theory. Trends are given to explain the effects of interfacial disorder.

II. EXPERIMENTAL DETAILS

Single-crystalline multilayers are grown on MgO(001) substrates by using MBE operating with a base vacuum of 8×10^{-9} Pa (6×10^{-11} torr). The MBE chamber is equipped with liquid nitrogen cryopanels, leading to working pressure equal to 3×10^{-9} Pa (2.5×10^{-11} torr). It should be noted that the vacuum pressure does not exceed 5×10^{-11} torr during Fe, Co, and Au growth or substrate heating. Prior to the deposition of the multilayers stack, the substrate is outgassed at 875 K and an additional 7-nm-thick MgO layer is grown at 725 K in order to improve the quality of the substrate surface, and more importantly to avoid the diffusion of residual carbon through the first Fe layer and its segregation at the surface.[9] A 50-nm-thick Fe layer is deposited at room temperature and annealed at 725 K for 20 min in order to obtain an atomically flat surface. Auger electron spectroscopy (AES) and XPS measurements reveal no traces of carbon contamination and sometimes the presence of oxygen traces, limited to less than 0.1 ML.

Subsequently, molecular oxygen is adsorbed at RT on this Fe(001) layer. O_2 is introduced by a leak valve with a partial pressure of 7×10^{-7} Pa (5×10^{-9} torr). The amount of adsorbed oxygen is controlled during the adsorption by monitoring the O 1*s* peak by XPS, which allows us to stop the adsorption when the desired coverage is reached. This process is performed in a separate chamber so as to avoid the oxidation of the crucibles and the deterioration of the high vacuum in the epitaxy chamber. XPS is done using standard Al/Mg anodes.

A structural analysis of oxygen overlayers is performed by using RHEED and STM. In addition to the surface lattice determination, the RHEED technique is employed to get information about the growth process (RHEED intensity oscillations) but also about in-plane lattice spacing variation. For this former purpose the evolution of RHEED profiles perpendicular to the $(0,-1)$, (0,0), and (0,1) diffraction streaks is recorded during the adsorption. The profiles are then fitted using Lorentzian line shapes, which allow us to extract the evolution of intensity, width, and position of each peak. STM imaging of Fe surfaces with different oxygen coverage is done in a chamber directly connected to the MBE chamber, in a pressure of 4×10^{-8} Pa (3×10^{-10} torr). These measurements are performed in the constant current mode. We use chemically etched *W* tips, which are heated under UHV by Joule effect and finally shaped above the sample surface by field effect prior to oxygen adsorption. In addition, the Fe oxidation state for the oxygen covered Fe(001) surface is investigated by XPS on MgO/Fe(50 nm)/Co(10 ML)/Fe(1 ML) multilayers.

The first steps of MTJs preparation is similar to what is described above (MgO buffer, 50-nm-thick Fe bottom electrode, using same annealing conditions). To prevent any contamination of the bottom Fe layer which may occur during STM experiments, the samples dedicated to transport measurements are not analyzed by STM. The controlled oxygen adsorption is performed on top of this bottom smooth Fe electrode and a 2.5-nm-thick MgO barrier is grown at RT. For this purpose we evaporate stoichiometric MgO by electron-beam heating at a growth rate between 0.01 and 0.02 nm/s. The MgO thickness is precisely controlled during the growth by monitoring RHEED intensity oscillations. Subsequently, a 15-nm-thick second Fe electrode is deposited on top of the MgO barrier. The whole stack is then annealed 10 min at 475 K. The hard/soft magnetic architecture in such a MTJ, necessary to operate independently the magnetization of its electrodes, is obtained by hardening the top Fe electrode by a 20-nm-thick Co overlayer. Samples are then capped with 20 nm of Au. After the growth, square MTJs with sizes varying from 10×10 to 200×200 μm^2 are patterned by optical lithography and ion etching.

III. O_2 ADSORPTION ON Fe(001)—RESULTS

A. Adsorption kinetics and growth mode

The O 1*s* peak area monitored by XPS during an adsorption run is plotted against the oxygen dose (1 Langmuir

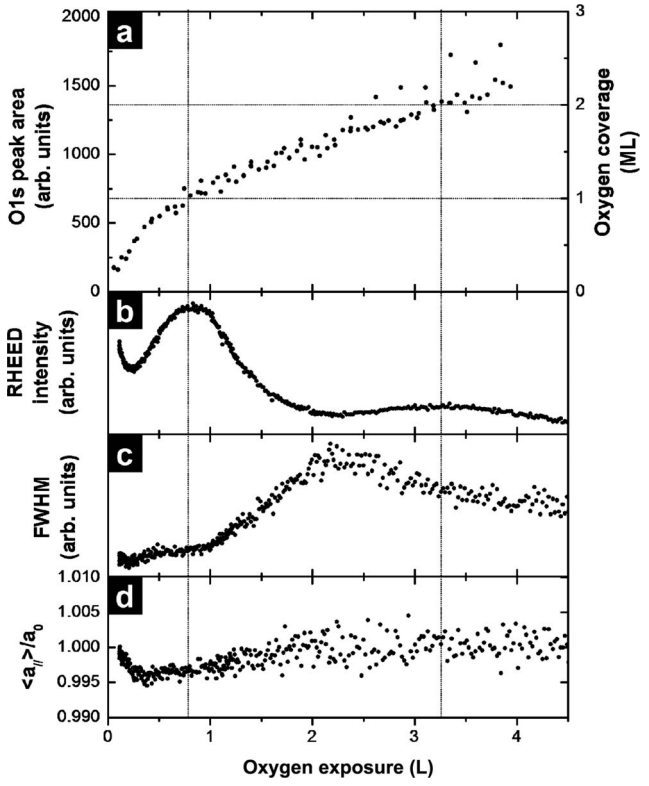

FIG. 1. (a) Area of the O 1*s* peak monitored by XPS during the adsorption of O_2 on Fe(001) (1 L $\equiv 10^{-6}$ torr s). Points from three experiments are plotted together and correspond to three different O_2 partial pressures (2.5×10^{-9}, 5.0×10^{-9}, and 7.5×10^{-9} torr). Right axis gives the corresponding oxygen coverage. (b) Intensity of the RHEED (01) diffraction rod. (c) FWHM of the (01) rod. (d) Relative variations in the surface in-plane lattice parameter.

$\equiv 10^{-6}$ torr s) in Fig. 1(a). For such low coverage the attenuation of photoelectrons by surface atoms can reasonably be neglected so that this area is almost proportional to the amount of deposited oxygen. The results of three separate adsorption processes are plotted together, corresponding to three different oxygen partial pressures: 2.5×10^{-9}, 5.0×10^{-9}, and 7.5×10^{-9} torr. Plotting the O 1*s* peak area versus the dose shows the superposition of the three kinetics. Thus, in this range the reaction rate is first order with respect to the pressure. Therefore the weak scatter reflects the good control and reproducibility of the process. The kinetics clearly exhibits the two regimes reported in previous studies.[27–32] The O 1*s* peak grows rapidly in the first stage up to a dose of 0.7 ± 0.1 L in our experimental conditions. Then the rate of adsorption decreases and keeps a constant value. In the literature it is not clear whether the transition between these two regimes corresponds to 0.5 ML (Refs. 27, 28, 30, and 31) or 1 ML (Refs. 29, 32, and 34) of adsorbed oxygen.

To complete the adsorption kinetics analysis, RHEED experiments are performed in real time during the oxygen adsorption process. Figures 1(b) and 1(c) show the (0,1) RHEED streak intensity and width, respectively, recorded during an adsorption process. The presence of two intensity oscillations probes a layer-by-layer growth. The first maximum, occurring at about 0.8 L, corresponds to the completion of the first monolayer and provides a calibration of the XPS measurements [see right axis in Fig. 1(a)]. As expected, the second maximum corresponds to a twice larger O 1*s* peak area. The quick decrease in the RHEED intensity can be attributed to the appearance of some roughness, structural disorder, or three-dimensional (3D) growth. The evolution of the (1,0) rod's full width at half maximum (FWHM) provides complementary information. Our observation is that the FWHM is nearly constant during the first oxygen monolayer deposition. This FWHM then increases up to 1.5 ML coverage and decreases for larger coverage. Such oscillating FWHM in opposite phase with intensity oscillations was reported in various cases of homoepitaxy and heteroepitaxy.[37] It has been shown to be related to the nucleation, growth, and coalescence of islands.[38] Figure 1(c) shows that the FWHM oscillation occurs during the second oxygen monolayer deposition. Interestingly, the nearly constant FWHM in the first adsorption regime indicates a different growth mode. Finally, the relative variations in the average in-plane lattice spacing parameter $\langle a_{\parallel}\rangle$ with respect to the initial substrate surface parameter a_0 are plotted in Fig. 1(d). They are extracted from the peaks positions in RHEED profiles, knowing that the distance between the $(0,-1)$ and (0,1) diffraction rods is inversely proportional to $\langle a_{\parallel}\rangle$. The measured $\langle a_{\parallel}\rangle$ does not deviates from the initial substrate value a_0 by more than 0.5%.

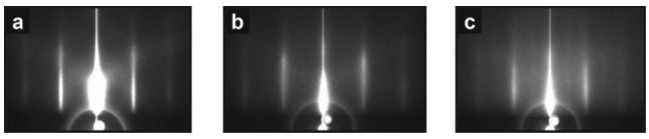

FIG. 2. RHEED patterns in azimuth [10] of Fe(001) surfaces with various adsorbed oxygen amounts. (a) 0 ML of oxygen (clean Fe), (b) 0.3, and (c) 2 ML.

B. Structure and morphology of oxygen covered Fe(001) surface

RHEED patterns of Fe(001) surfaces with various oxygen coverages are shown in Fig. 2. For a clean Fe surface, RHEED patterns are highly contrasted with thin diffraction rods and marked Kikuchi lines. The background intensity gradually increases during the adsorption, indicating an increasing surface disorder. For sufficiently high oxygen coverage (>2 ML) low-intensity additional streaks appear in the RHEED pattern, typical of a new crystalline structure.

STM images shown in Fig. 3 illustrate the morphology of oxidized Fe(001) surfaces at a large scale (200×200 nm^2). Concerning clean Fe(001) one can see large terraces bordered by monatomic steps. These steps are curved and often link two threading dislocations or holes. We ascribe the latter to some dewetting (since Fe growth on MgO forms 3D islands at equilibrium). It should be noted that the atomic resolution is not reached at RT. Surprisingly, surfaces with less than 1 ML of oxygen are similar. The presence of oxygen is thus not directly evidenced by STM in this first adsorption regime. Adsorbing more than 1 ML results in the formation of oxide islands. These islands are uniformly distributed and appear as bright regions in STM images. The islands cover-

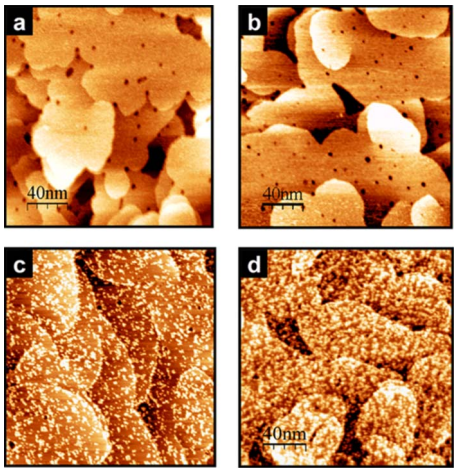

FIG. 3. (Color online) 200×200 nm^2 STM images of Fe(001) surfaces with various adsorbed oxygen amounts (tip-sample voltage: −500 mV and current: 1 nA). (a) 0 ML of oxygen (clean Fe), (b) 0.3, (c) 1.2, and (d) 2 ML.

age estimated from Fig. 3(c) is found to be around 30% of the whole surface. An important point is that the atomic resolution is now attained at RT (Fig. 4). The observed islands are one atom high and lie on a square surface lattice whose parameter is 0.29 nm, that is, the parameter of the Fe(001) surface. The atoms which compose these islands are found to be on top of the underlying atoms.

The atomic resolution obtained for coverage above 1 ML is an opportunity to observe additional adsorption mechanisms. Indeed, many clusters composed of four surface atoms appear darker than the surrounding lattice in atomic scale images (Fig. 4). Moreover, these square depletions are found to move when recording several successive STM images. No correlation has been observed between their trajectory and the STM tip movements. From the extracted profiles along these features, the induced vertical displacements of the tip reach 0.06 nm in our tunneling conditions. We ascribe these features to isolated oxygen adatoms. O and N atoms, which are highly electronegative and hence have strong interactions with a metallic substrate, are known to appear as depressions.[39–41] On our Fe(001) surfaces we identify the

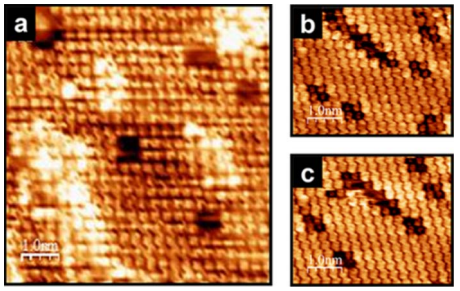

FIG. 4. (Color online) STM images of the Fe(001) surface with 1.2 ML of oxygen shown in Fig. 3(c) (tip-sample voltage: −500 mV and current: 1 nA). In (a) one can see oxide islands and square depletions lying on a $p(1\times1)$-O lattice. The mobility of the square depletions is illustrated in (b) and (c), which are two images of the same area recorded at a few seconds of interval.

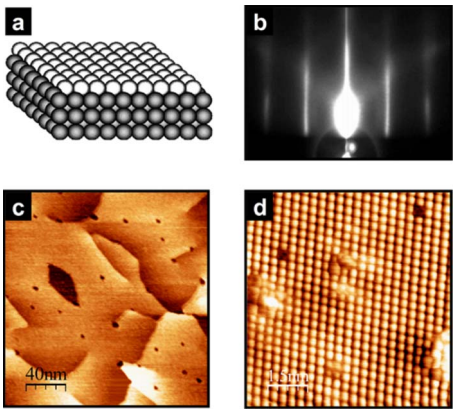

FIG. 5. (Color online) $p(1\times1)$-O reconstruction on Fe(001), (a) sketch of the surface, (b) RHEED pattern in (Ref. 10) azimuth, (c) 200×200 nm^2 STM image of the surface, and (d) atomically resolved 7.6×7.6 nm^2 STM image (tip-sample voltage: −500 mV and current: 1 nA).

species to oxygen since no other species are detected by XPS and AES. The square shape of these features is direct evidence that isolated oxygen adatoms are located in the hollow site. They equally alter the local density of states of the four underlying Fe atoms.

C. Temperature driven $p(1\times1)$ ordering

Flashing oxidized Fe(001) at 925 K leads to the recovery of very flat surfaces, as shown in Fig. 5. The RHEED pattern remains unchanged up to about 675 K. A reordering of the surface then occurs (not shown here). At 925 K the RHEED pattern becomes very similar to a clean Fe(001) one [Fig. 5(b)] and shows no change at higher temperatures. All the eventual additional streaks due to oxide islands completely disappear and the contrast strongly increases, which indicates a $p(1\times1)$ ordering of the surface. It should be noted that the oxygen coverage must not be too high to recover such a RHEED pattern. When the amount of oxygen exceeds the equivalent of 2 ML we observe that the diffraction rods' intensity remains modulated along their length.

Large scale STM images of $p(1\times1)$ reconstructed surfaces confirm the complete disappearance of islands and look like preoxidized Fe(001) surfaces [Fig. 5(c)]. In addition, Fe-O bonding makes the atomic resolution attainable at RT. Observations at this scale evidence the presence of a continuous atomic surface layer and confirm the $p(1\times1)$ reconstruction [Fig. 5(d)]. Whatever the initial oxygen amount is (between 1 and 2 ML), the O 1*s* peak area measured by XPS after annealing corresponds to 1 ML.

D. Fe oxidation state at the surface

Figure 6 shows Fe 2*p* spectra recorded during the oxygen adsorption on a MgO/Fe(50 nm)/Co(10 ML)/Fe(1 ML) multilayer. The Co layer was used in order to enhance the sensitivity to the Fe surface plane. Clear RHEED intensity oscillations were observed during the growth of Co and of the top Fe layer, demonstrating a low roughness of the films and a good covering of the top Fe. As probed by RHEED

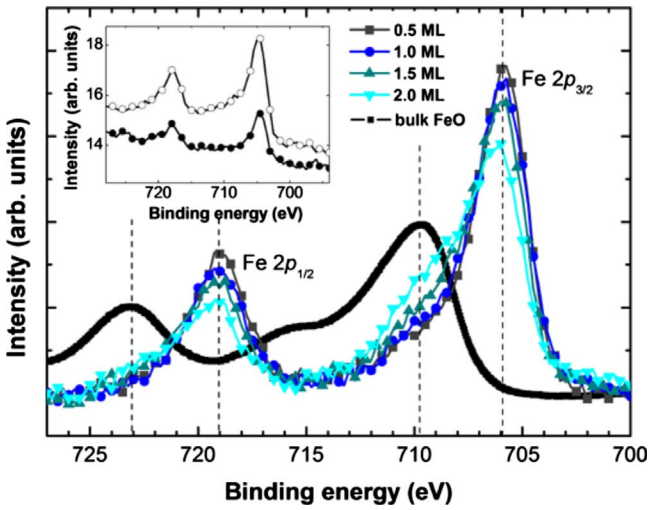

FIG. 6. (Color online) Evolution of the Fe $2p$ peaks measured by XPS during O_2 adsorption on MgO/Fe(50 nm)/Co(2.8 nm)/Fe(1 ML). The reference line for bulk FeO is from Ref. 32. Inset: Fe $2p$ XPS signal on substrate MgO/Fe(50 nm)/Co(2.8 nm) (filled circles) and substrate MgO/Fe(50 nm)/Co(2.8 nm)/Fe(1 ML) (empty circles).

patterns, the surface lattice remained square. Therefore, the Co layer does not significantly alter the Fe structure. Moreover, the adsorption kinetics particular to the $Fe(001)/O_2$ system and depicted in Fig. 1 are identical when adsorbing O_2 on Fe/Co(10 ML)/Fe(1 ML). Consequently, the XPS measurements carried out on the latter surface can reasonably be extended to the oxygen adsorption on 50-nm-thick Fe(001) films.

As evidenced by the curves shown in the inset of Fig. 6, the Co film strongly attenuates the signal due to photoelectrons excited in the Fe buffer, in such a way that about half of the Fe $2p$ signal is then due to the topmost Fe monolayer. The Fe $2p_{1/2}$ and $2p_{3/2}$ binding energies are measured, respectively, at 719 and 706 eV. During adsorption, a slight shift of the Fe $2p_{3/2}$ core level to a higher energy is observed but is not distinguished on the Fe $2p_{1/2}$ level. The intensities of both peaks gradually decrease while shoulders grow at 723 and 710 eV, especially after the completion of the first oxygen monolayer. These shoulders are typical of an iron oxide phase. Moreover, the shift of the Fe $2p$ peaks suggests that this phase is close to FeO rather than Fe_2O_3 and Fe_3O_4 phases.

E. O_2 adsorption on Fe(001)—general discussion

The presence of two regimes in the adsorption kinetics monitored by XPS is in agreement with previous studies.[27–32] RHEED intensity oscillations clearly demonstrate that the transition between the two adsorption regimes occurs at 1 ML of oxygen. This is perfectly supported by the O $1s$ peak intensity due to the $p(1\times1)$ reconstruction obtained after annealing. It has been suggested that the two first oxygen monolayers deposition proceeds in a layer-by-layer growth[27] before the 3D growth of bulklike oxide.[27,35] We confirm this assumption by the observation of RHEED intensity oscillations and by the appearance of two-dimensional islands after the completion of the first oxygen monolayer.

We now focus our discussion on the *first oxygen monolayer adsorption*. To account for the kinetic behavior, Simmons and Dwyer[27] proposed a mechanism involving a mobile precursor, presumed to be molecular oxygen in a very low concentration (not detectable by XPS or Auger spectroscopy). It was expected to mediate the chemisorption at every stage of adsorption, that is, both on the initial clean Fe(001) surface and on the subsequently grown overlayers. Indeed, STM imaging gives direct proof that a mobile species exists during the second oxygen layer adsorption (appearing as square depletions, see Fig. 4). However, we identify it with atomic oxygen rather than O_2, which is consistent with the fact that the presence of O_2 has never been evidenced in previous studies. In the first monolayer adsorption, such mobile oxygen adatoms are not evidenced by STM. This is not surprising because their presence tends to lower the apparent atomic corrugation, which is not resolved on clean Fe(001) at RT. Our results suggest that the first monolayer is initially composed almost entirely of this precursor since no island is seen with STM and since the FWHM of RHEED streaks remains constant. This also contradicts the rise and growth of $c(2\times2)$ patches sometimes reported[27,28] and certainly due to C contamination. This first phase is thus in a disordered/gas phase, as confirmed by the increasing background observed in RHEED patterns during this first regime. The nature of this disorder has already been investigated by means of high-resolution electron energy-loss spectroscopy.[34] It was clearly shown that atomic oxygen preferentially adsorbs on the four-fold hollow sites, and partially populates the bridging and on-top sites when approaching the full coverage. This probably leads to the adsorption rate slowdown we measure with XPS between 0.5 and 0.7 L. Nevertheless, to account for the temperature dependence of the O_2 adsorption kinetics, Brundle[30] inferred that the degree of ordering should be quite high at RT. Our STM experiments support this assumption since a $p(1\times1)$-O reconstruction is seen after the completion of the first oxygen layer.

In the *second monolayer adsorption*, the additional oxygen is adsorbed on this $p(1\times1)$-O layer into the mobile precursor state. In parallel, the nucleation and growth of oxide islands take place. The islands uniformly cover the surface and are separated by a few Angströms as indicated by the evolution of the FWHM and probed by STM. In agreement with published results,[28,33,35] XPS shows that this initial oxide is mainly composed of Fe^{2+}. Having established the FeO nature of the islands, their coverage measured from STM large scale images [0.3 ML from Fig. 3(c)] is in agreement with the 1.2 ± 0.1-ML-thick oxygen deposition fixed with XPS assuming that the film is constituted of a $p(1\times1)$ oxygen phase plus 0.2 ± 0.1 ML corresponding to islands. Knowing that the lattice constant of bulk FeO in the cubic wustite phase with the NaCl structure is 0.431 nm, one can expect an epitaxy relationship similar to the one of the Fe/MgO(001) system, that is, Fe(001)[100]/FeO(001)[110]. This means that the atoms composing islands seen in Fig. 4 and located in the on-top sites of the $p(1\times1)$ are Fe atoms. O atoms of the islands are not resolved. Since $\langle a_{\parallel}\rangle$ extracted from RHEED patterns remains close from the Fe(001) sub-

strate value within ±0.5%, the growth of the initial oxide islands is pseudomorphic for the investigated coverage. Furthermore, the increasing background intensity of RHEED patterns and the rapid decrease in the diffraction streaks intensity are due to the inhomogeneity of the surface at small scale. The appearance of new diffraction streaks for coverages greater than 2 ML probes a new crystallographic phase. It was shown that an Fe_xO/Fe_2O_3 mixed oxide layer grows on top of the FeO layer at this stage.[33]

The ordering of the surface obtained thanks to annealing at 925 K leads to a complete oxygen monolayer entirely reconstructed in a $p(1\times1)$ fashion. Previous studies showed that the (i) oxygen surplus diffuses into the bulk, (ii) oxygen occupies Fe(001) hollow sites only,[34] and (iii) the eventual amount of Fe^{3+} species strongly decreases.[33] The stability of this phase was also shown,[36] which explains why oxygen tends to form a $p(1\times1)$ layer even without annealing. However, only a high-temperature annealing provides the homogeneous ordering over the whole surface and the recovery of highly contrasted RHEED patterns.

Both ordered and disordered Fe(001)/O surfaces are interesting. Indeed, the spin-polarized transport in single-crystal Fe/MgO/Fe MTJs is strongly linked to the crystalline symmetries and therefore to the degree of order. Here the term "disorder" combines all the small scale inhomogeneities of chemical composition and structure (in particular, oxide islands) which disturb the perfect crystalline periodicity of the Fe(001) surface. Therefore, the ordered $Fe/p(1\times1)$-O/MgO interface allows us to investigate the role of interfacial chemical bonds, whereas in MTJs with nonannealed interfacial oxygen layers the effects of both chemical bonds and disorder should arise.

IV. Fe/FeO/MgO/Fe(001) MAGNETIC TUNNEL JUNCTIONS

A. MTJs growth

Given the level of understanding we aim at, a detailed analysis of the MgO growth on top of the oxygen overlayer is required before discussing the magnetotransport measurements. For this purpose, we performed RHEED intensity oscillations during the MgO deposition on disordered and ordered oxygen layers prepared on Fe(001), and compared them to the RHEED oscillations obtained on the clean Fe(001) surface. The results are shown in Fig. 7. The layer-by-layer growth mode adopted by MgO on Fe(001) is clearly not affected by the presence of oxygen. The only small difference is that the amplitude of RHEED oscillations is a little smaller on disordered oxygen layers, compared to clean Fe(001) and $p(1\times1)$-O surfaces. This is not surprising since RHEED intensity oscillations are very sensitive to any disorder. However, the RHEED patterns observed on 2.5-nm-thick deposited MgO barrier on these three different initial surfaces are similar. The crystalline quality of the MgO barrier is thus not strongly affected according to the observed RHEED patterns. We should mention that the growth of MgO onto clean Fe(001) and $p(1\times1)$-O surfaces was further investigated by Cattoni *et al.*,[42] who found a beneficial influence of the oxygen layer on the crystallinity of MgO and on the quality of the interface.

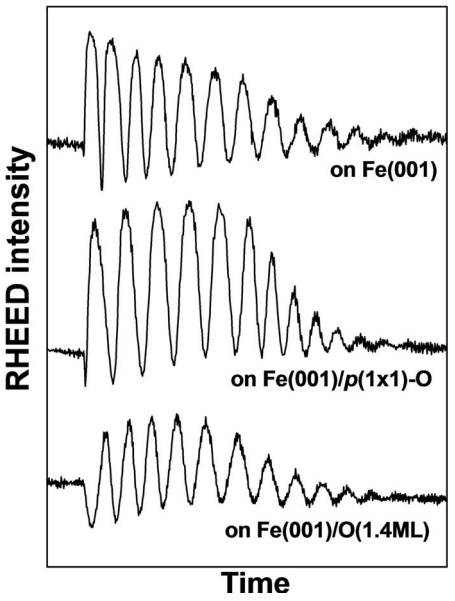

FIG. 7. RHEED intensity oscillations recorded during the layer-by-layer growth of MgO at RT on three initial surfaces.

Furthermore, we checked by using XPS that the adsorbed oxygen layer is not removed upon MgO deposition. To demonstrate it experimentally, two samples were first grown: (i) a $Fe/p(1\times1)$-O surface and (ii) an Fe(001) clean surface. The O 1*s* peak was then measured by XPS on both samples. The second step was to grow one MgO atomic plane on both samples in the same process and to measure again the O 1*s* peak by XPS. The observations are very clear. First, the O 1*s* peak corresponding to 1 ML of MgO grown on $Fe/p(1\times1)$-O is found to be equal to the sum of the peaks measured on the one hand on Fe/MgO(1 ML) and on the other hand on the $Fe/p(1\times1)$-O surface, taking into account for the latter the attenuation of photoelectrons by an atomic layer of MgO. For this treatment, the attenuation length of O 1*s* photoelectrons (0.84 nm for a kinetic energy of about 960 eV) was extracted from measurements of the O 1*s* peak after successive depositions of MgO monolayers. Second, Mg 1*s* peaks with identical shapes and areas are measured on both samples. This experiment clearly means that (i) the adsorbed oxygen is not consumed by the MgO growing layer itself and (ii) the adsorbed oxygen does not segregate on top of the MgO layer. The MgO deposition thus does not alter the adsorbed oxygen layer.

In standard Fe/MgO/Fe MTJs, the second Fe electrode is deposited on the MgO barrier at RT and the whole stacking is then annealed at 675 K during 20 min. This annealing is absolutely necessary to obtain the highest TMR values reported on the Fe/MgO/Fe(001) system (180% at RT). This process is however not suitable for MTJs with disordered oxygen at the Fe/MgO interface since the oxygen overlayer on Fe(001) begins to reorder at this temperature. Consequently, we have limited this annealing to 10 min at 475 K. For this reason, the maximum TMR value obtained for clean interfaces reaches 140% and the results obtained with oxygen have to be compared to this value.

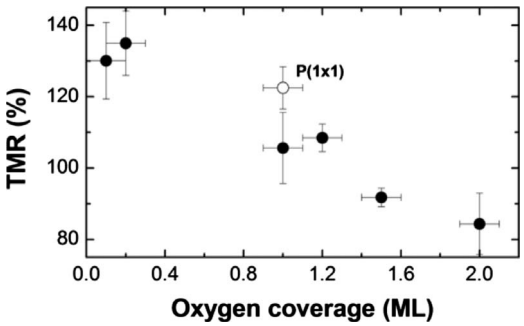

FIG. 8. TMR of Fe/O/MgO/Fe(001) MTJs measured at 10 mV at RT versus oxygen content adsorbed at the Fe/MgO bottom interface. Solid symbols: MTJs with a nonannealed FeO interfacial layer (disordered interface). Open symbol: MTJ with an annealed FeO interfacial layer [$p(1\times1)$ reconstructed].

B. Magnetotransport results

The magnetotransport experiments are performed on MTJ stacks with MgO barrier thickness of 2.5 nm. This corresponds to the asymptotic regime[2] where the dominant propagating wave functions have a wave vector normal to the barrier and symmetries are those with the smaller attenuation rate within the MgO.

The evolution of the TMR at zero bias with the interfacial oxygen content is plotted in Fig. 8. Vertical error bars represent the standard deviation obtained from the measure of 22 MTJs on every sample. The larger the oxygen amount, the lower is the MR ratio. For disordered interfaces, the TMR is 110% at 1 ML. MTJs containing the $p(1\times1)$-O reconstruction present ratios beyond 120%.

We systematically investigate the bias dependence of the TMR and of the conductance in both P and AP configurations of magnetizations. The voltage is defined with respect to the top electrode, which means that in positive bias electrons flow from the bottom oxidized interface to the top one. Figure 9 shows the evolution of the TMR(V) for various oxygen coverage rates. To allow their comparison, the curves are normalized to their maximum value, which is always measured at 0 V. The TMR of standard Fe/MgO/Fe(001) MTJs is highly asymmetric, as reported in previous studies.[6,8] When increasing the oxygen content it gets gradually more symmetric. This is associated with a relative decrease in the TMR at both negative and positive biases. However it is evident that the main changes occur for positive voltage. This TMR reduction is found to be gradual when increasing the oxygen content and stronger with the $p(1\times1)$-O interfacial layer.

Figure 10 displays the normalized conductances of oxygen-doped MTJs at low bias for P and AP configurations. Conductances over a wider voltage range are shown in Fig. 11 for the Fe/MgO/Fe and Fe/$p(1\times1)$-O/MgO/Fe MTJs. The first observation is that the presence of oxygen *does not* make the conductances symmetrical with respect to the bias. Therefore, the fact that the TMR(V) curve becomes symmetric is purely fortuitous and should not lead to the conclusion that the top MgO/Fe interface is oxidized. The relative reduction in the TMR at positive bias is clearly due to a strong reduction in the parallel conductance G_P while the antiparallel one G_{AP} remains almost unaffected by interfacial oxygen. At negative bias both G_P and G_{AP} seem to increase. The inflection of G_{AP} at about −0.2 V remains. The conductance evolution is gradual when increasing the oxygen amount. However, when the interfacial oxygen coverage exceeds 2 ML the low-bias structure of G_P and G_{AP} completely disappears. The conductances become parabolic, as shown for G_P in Fig. 12. However, the TMR still reaches 85% in this case.

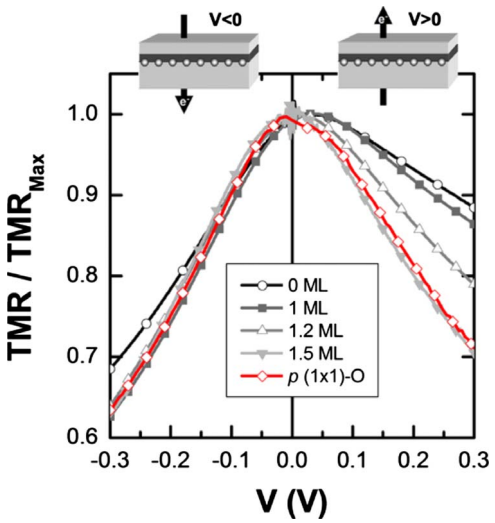

FIG. 9. (Color online) Normalized TMR versus applied voltage for several Fe/O/MgO/Fe(001) MTJs with various oxygen contents at the bottom Fe/MgO interface (the voltage sign is defined with respect to the top electrode).

C. Discussion

Zhang *et al.*[11] computed the expected effect of interfacial oxygen on the TMR of epitaxial Fe/MgO/Fe MTJs at zero bias. They found that the TMR should drop exponentially, loosing 1 order of magnitude for a coverage of 1 ML. Their theoretical TMR values reached about 4000% for an ideal MTJ and 100% for an Fe/$p(1\times1)$-O/MgO/Fe MTJ, considering an 8-ML-thick barrier. Higher ratios are expected for larger thicknesses. Thus it is often claimed that interfacial oxygen is responsible for the limited measured TMR. Our experiments clearly do not confirm such a huge detrimental effect. Qualitatively, we actually measure a sizable and monotonous decrease, which illustrates again the sensitivity of spin-polarized transport to interfaces. Even though a quantitative agreement is not reached with *ab initio* calculations, the analysis performed by Zhang *et al.*[11] provides useful clues for interpreting our results. This will be addressed first through the comparison of Fe/MgO/Fe(001) and Fe/$p(1\times1)$-O/MgO/Fe(001) MTJs; then the influence of disorder will be discussed.

We first want to discuss about the Fe-O bonding influence on the electronic transport. In Ref. 11 it is demonstrated that at zero bias, the Fe-O bonds have a much higher impact on the majority-spin tunneling current than on the minority-spin current. This leads to a strong reduction in G_P while G_{AP} is weakly affected. Our measurements agree with this since the TMR decrease we observe here is due to the reduction in G_P.

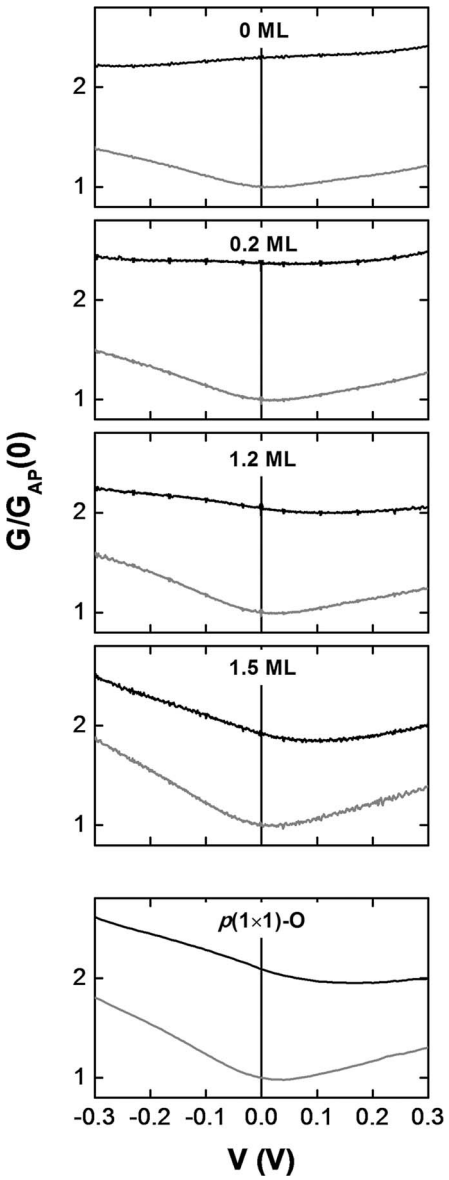

FIG. 10. Normalized dI/dV conductances in the parallel (black) and antiparallel (gray) configurations of magnetization, for several Fe/O/MgO/Fe(001) MTJs with various oxygen contents at the bottom Fe/MgO interface.

The origin of this phenomenon was shown to be the charge transfer from Fe to O in the interfacial plane. The Fe Δ_1 density of states (DOS) at the Fermi level becomes strongly localized within the FeO plane, mainly through s and p orbitals. This in turn reduces the matching of the Δ_1 wave

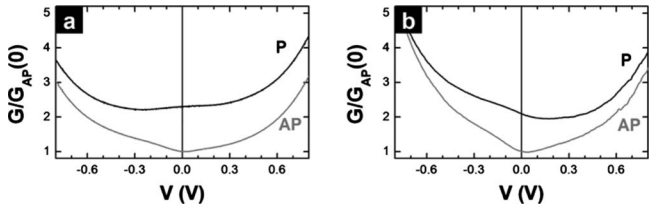

FIG. 11. Normalized dI/dV conductances in the P and AP configurations of magnetization. (a) Fe/MgO/Fe(001) and (b) Fe/$p(1\times1)$-O/MgO/Fe(001).

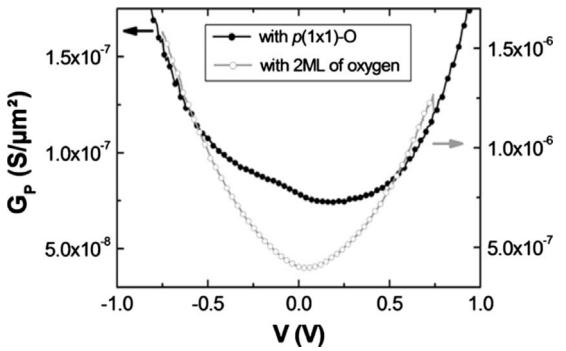

FIG. 12. Parallel conductances of two MTJs with different oxidized bottom Fe/MgO interfaces: Fe/$p(1\times1)$-O/MgO/Fe MTJ with an highly ordered interface (black) and Fe/O(2 ML)/MgO/Fe with an highly disordered interface (gray).

functions with the available tunneling states in MgO and therefore their injection in the barrier. As an experimental clue, this localization of the Fe interfacial DOS allows us to reach a higher lateral resolution with STM on the Fe/$p(1\times1)$-O surface than on clean Fe(001), where electrons are highly delocalized at RT. Now we turn to the bias dependence of the conductances. In a simple picture of tunneling, electrons from one electrode scan the empty DOS of the opposite interface. Therefore, the fact that the experimental G_P reduction at 0 V extends to positive bias means that the occupied majority states at the bottom Fe/MgO interface are involved more importantly than the empty states. Theoretical efforts have been done to compute the bias dependence of TMR in epitaxial MTJs.[18–20] The presence of oxygen at the interfaces has also been considered. Different behaviors arise from these studies. According to Ref. 18, the TMR should be almost zero at zero bias and should increase with increasing the voltage. From Ref. 19, an Fe/$p(1\times1)$-O/MgO/Fe MTJ should exhibit a negative TMR over the whole voltage range considered here, the TMR decreasing continuously when increasing the bias. Obviously, we observe none of these scenarios. However, both theoretical studies point out that in Fe/$p(1\times1)$-O/MgO/Fe MTJs G_{AP} should be much more sensitive to the bias than G_P because of interface resonant states (IRS) contributions. In particular, the main feature in the conductances predicted in Ref. 19 is a strong increase in G_{AP} correlated with the activation of an unoccupied IRS at the FeO/MgO interface. This has been predicted to occur at about −0.5 V for a 12-ML-thick MgO barrier[43] (with our convention for the voltage sign) and may be the key point for interpreting the relative increase we observe at negative bias (further experimental investigations are in progress). However, the overall matching between measured and computed voltage dependences remains doubtful. As was suggested in Refs. 18 and 24, IRS-induced features in the conductances are certainly less sharp in practice than in theory because of roughness or local defects. That is why theoretical studies including a proper modeling of defects[25] are maybe more suited to real Fe/MgO/Fe(001) MTJs.

Another important result obtained in this study concerns the effect of interfacial disorder on the conductance. Both Fe/MgO/Fe and Fe/$p(1\times1)$-O/MgO/Fe MTJs present a high degree of order (bulk and interface). On the other hand,

in comparison the bottom oxidized Fe/MgO interface of the MTJs without $p(1\times1)$ reconstruction presents local order combined with long-range disorder, as shown in the first part of this paper (see Fig. 3). Therefore, they present a mixed effect of both Fe-O bonding and disorder. Let us recall that disorder means here any disturbance of the crystalline periodicity at the interface induced by adsorbed O_2. Therefore this includes first the presence of some oxygen atoms possibly located in bridge or on-top sites of Fe(001) (Ref. 34) and second the presence of FeO islands. Indeed, the islands edges, the possible imperfect stoechiometry of these islands and finally the induced interfacial roughness participate to disorder. We must mention that the MgO still grows layer-by-layer on disordered oxidized Fe(001) surfaces, as evidenced by RHEED intensity oscillations. However we cannot rule out that the bottom interfacial disorder also induces some disorder in the barrier or an increased roughness of it. It is clear that the $G_{P/AP}(V)$ characteristics and TMR values are different for the same oxygen content, whether the oxidized Fe layer was annealed (ordered) or not. As shown in Fig. 9, the TMR reduction at positive bias characteristic of Fe-O bonding is gradual when increasing the interfacial oxygen amount but is surprisingly less pronounced when the interface is disordered. Thus, one could expect higher TMR than in Fe/$p(1\times1)$-O/MgO/Fe MTJs. This is actually not the case; it is shown in Fig. 8 that the TMR in MTJs with a disordered interface is lower than in ordered ones. This shows that in these MTJs the TMR is also reduced by local inhomogeneities which break the crystalline periodicity at the interface. This reduction seems to have almost the same amplitude than the reduction induced by Fe-O bonding; it is certainly not negligible but it does not completely suppress the TMR. This detrimental effect of disorder is an additional indication that the TMR is dependent on the crystal and electronic Bloch states symmetry conservation both within the bulk and across the interfaces.[2] Note that even though oxidized surfaces are not as flat and homogeneous at a small scale as the clean Fe(001) one, STM and RHEED experiments probe that the order remains relatively high. This could explain why the TMR is not drastically reduced. On the other hand, this means that a limited interfacial disorder has sizable effects on the TMR. Consequently, one can extrapolate our results and suspect that in real Fe/MgO/Fe(001) MTJs any deviation from the ideal stacking will have such a detrimental effect on spin-polarized transport. Hence, the cumulated effects of local defects at both sides of the barrier (for instance, interfacial misfit dislocations and edge terraces) could possibly explain the quantitative discrepancies between theory and experiments concerning the TMR ratio amplitude.

For large oxygen amounts G_P becomes parabolic (Fig. 12), which strongly suggests two hypotheses: (i) one looses the electronic structure signature on the transport of bcc Fe. The measured large TMR ratio (85%) above the free-electron expectation having in view the bulk polarization of Fe invalidates this first hypothesis[5] and (ii) interfacial diffusion of the bulk wave function determines a free-electronlike parabolic conductance response. It is obvious that interfacial disorder should enhance diffusive phenomena. Local defects (isolated atoms or island edges) break the crystalline symmetry, in such a way that electrons experience local variations in the periodic potential and can be elastically scattered. As a result, a pure symmetry in the bulk will be described at the interface by a linear combination of all the other symmetries (Δ_i) with different amplitudes. However, in our junctions with 2.5-nm-thick MgO barriers having in view the symmetry-dependent attenuation rate within the single-crystal MgO barrier only mostly freelike s electrons (Δ_1 symmetry whose attenuation rate is the smallest within the MgO) are dominant in the tunneling. This hypothesis is supported furthermore by the parabolic shape of G_{AP} that suggests the opening of a Δ_1 channel in the AP state. Therefore in the AP configuration, Δ_1 majority states which are propagative wave in one electrode and evanescent one in the other can be scattered at the interface into a propagative state and then participate to tunneling.[25] In this simple scheme the scattering rate (reflected by the probability amplitude of the Δ_1 component of the wave function at the interface) determines the amplitude of the TMR. In our case it would be large enough to observe parabolic conductance but low enough to keep a large TMR (85%). At this point we propose only simple trends to understand these observations, more sophisticated theoretical calculation being necessary to get more insight.

V. CONCLUSION

To investigate experimentally the effect of interfacial oxygen in Fe/MgO/Fe(001) MTJs, we have studied in details the mechanisms of oxygen adsorption on Fe(001). With respect to similar experiments performed by several groups before, the present work allows us to go further into the understanding of the adsorption kinetics and the role of the interfacial order and chemical structure on spin-polarized tunneling transport in MTJs. Our experimental observations shown here are in agreement with previous works. However, in addition, we definitely clarify two important points. First, using STM and also quantitative information given by RHEED (intensity oscillations, FWHM, and in-plane lattice spacing oscillations) we demonstrate that the coverage ratio at which the adsorption kinetics change corresponds to exactly 1 ML of adsorbed oxygen. Second, the STM and RHEED analysis clearly demonstrates that the adsorption kinetics modification at this coverage is due to a phase transition from a disordered to a condensed phase. This condensed phase is constituted of FeO islands, whereas a $p(1\times1)$ oxygen phase is observed on the rest of the surface. This surface oxygen ordering, strongly suggested in previous works, is clearly demonstrated here. Moreover, as an annealing process was known to get such a $p(1\times1)$ oxygen surface lattice, the STM observations on such a prepared surface definitely confirm this ordering.

This detailed analysis on oxygen adsorption allowed us to build Fe/MgO/Fe(001) MTJs with controlled amount of oxygen and order/disorder at interface. This led to a complex study on correlation between oxygen interfacial doping and order/disorder and spin-polarized tunneling/symmetry filtering effects in single-crystal MTJs. Comparing MTJs having a highly ordered bottom interface [Fe/MgO/Fe and Fe/$p(1\times1)$-O/MgO/Fe], we have shown that interfacial Fe-O

bonds lower the parallel conductance, in agreement with *ab initio* calculations. This effect is asymmetric with respect to bias, which means that oxygen principally affects the occupied states of Fe at the interface. In MTJs with a disordered FeO interfacial layer, the signature of Fe-O bonds on the parallel conductance appears gradually when increasing the oxygen amount. In addition, the increasing disorder alters the fine structure of conductances, suggesting a predominant tunneling of *s* electrons due to scattering at the interface. Both Fe-O bonds and interfacial disorder slightly reduce the TMR. However, from a reference value of 140% in Fe/MgO/Fe, the TMR drops to 120% in Fe/$p(1\times1)$-O/MgO/Fe and still reaches 85% with a disordered 2 ML FeO interface. This clearly means that any oxygen contamination during the process of Fe/MgO/Fe growth by MBE or sputtering is not as harmful to the TMR amplitude as suggested by the calculations within nondiffusive models. Consequently, the discrepancy between the 1000% theoretical TMR and the 180% experimental results at RT for this particular Fe/MgO/Fe(001) system cannot be strictly assigned only to interfacial oxygen contamination.

ACKNOWLEDGMENTS

The authors would like to thank F. Montaigne and B. Kierren for their help in lithography process and STM experiments, respectively.

[1] S. S. P. Parkin, C. Kaiser, A. Panchula, P. M. Rice, B. Hughes, M. Samant, and S.-H. Yang, Nature Mater. **3**, 862 (2004).
[2] W. H. Butler, X.-G. Zhang, T. C. Schulthess, and J. M. MacLaren, Phys. Rev. B **63**, 054416 (2001).
[3] J. Mathon and A. Umerski, Phys. Rev. B **63**, 220403 (2001).
[4] M. Bowen, V. Cros, F. Petroff, A. Fert, C. Martínez Boubeta, J. L. Costa-Krämer, J. V. Anguita, A. Cebollada, F. Briones, J. M. de Teresa, L. Morellón, and M. R. Ibarra, Appl. Phys. Lett. **79**, 1655 (2001).
[5] J. Faure-Vincent, C. Tiusan, E. Jouguelet, F. Canet, M. Sajieddine, C. Bellouard, E. Popova, M. Hehn, F. Montaigne, and A. Schuhl, Appl. Phys. Lett. **82**, 4507 (2003).
[6] S. Yuasa, T. Nagahama, A. Fukushima, Y. Suzuki, and K. Ando, Nature Mater. **3**, 868 (2004).
[7] S. Ikeda, J. Hayakawa, Y. Ashizawa, Y. M. Lee, K. Miura, H. Hasegawa, M. Tsunoda, F. Matsukura, and H. Ohno, Appl. Phys. Lett. **93**, 082508 (2008).
[8] C. Tiusan, M. Sicot, J. Faure-Vincent, M. Hehn, C. Bellouard, F. Montaigne, S. Andrieu, and A. Shuhl, J. Phys.: Condens. Matter **18**, 941 (2006).
[9] M. Sicot, S. Andrieu, C. Tiusan, F. Montaigne, and F. Bertran, J. Appl. Phys. **99**, 08D301 (2006).
[10] H. L. Meyerheim, R. Popescu, J. Kirschner, N. Jedrecy, M. Sauvage-Simkin, B. Heinrich, and R. Pinchaux, Phys. Rev. Lett. **87**, 076102 (2001).
[11] X. G. Zhang, W. H. Butler, and A. Bandyopadhyay, Phys. Rev. B **68**, 092402 (2003).
[12] S. G. Wang, G. Han, G. H. Yu, Y. Jiang, C. Wang, A. Kohn, and R. C. C. Ward, J. Magn. Magn. Mater. **310**, 1935 (2007).
[13] K. Miyokawa, S. Saito, T. Katayama, T. Saito, T. Kamino, K. Hanashima, Y. Suzuki, K. Mamiya, T. Koide, and S. Yuasa, Jpn. J. Appl. Phys., Part 1 **44**, L9 (2004).
[14] L. Plucinski, Y. Zhao, B. Sinkovic, and E. Vescovo, Phys. Rev. B **75**, 214411 (2007).
[15] P. Luches, S. Benedetti, M. Liberati, F. Boscherini, I. I. Pronin, and S. Valeri, Surf. Sci. **583**, 191 (2005).
[16] C. Li and A. J. Freeman, Phys. Rev. B **43**, 780 (1991).
[17] B. D. Yu and J.-S. Kim, Phys. Rev. B **73**, 125408 (2006).
[18] C. Zhang, X. G. Zhang, P. S. Krstic, H. P. Cheng, W. H. Butler, and J. M. MacLaren, Phys. Rev. B **69**, 134406 (2004).
[19] C. Heiliger, P. Zahn, and I. Mertig, J. Magn. Magn. Mater. **316**, 478 (2007).
[20] C. Heiliger, P. Zahn, B. Y. Yavorsky, and I. Mertig, Phys. Rev. B **73**, 214441 (2006).
[21] R. Guerrero, D. Herranz, F. G. Aliev, F. Greullet, C. Tiusan, M. Hehn, and F. Montaigne, Appl. Phys. Lett. **91**, 132504 (2007).
[22] C. Tiusan, M. Sicot, M. Hehn, C. Bellouard, S. Andrieu, F. Montaigne, and A. Schuhl, Appl. Phys. Lett. **88**, 062512 (2006).
[23] H. Itoh, J. Phys. D **40**, 1228 (2007).
[24] J. P. Velev, K. D. Belashchenko, and E. Y. Tsymbal, Phys. Rev. Lett. **96**, 119601 (2006).
[25] X. G. Zhang, Y. Wang, and X. F. Han, Phys. Rev. B **77**, 144431 (2008).
[26] F. Bonell, A. M. Bataille, S. Andrieu, C. Tiusan, B. Kierren, G. Lengaigne, and D. Lacour, Eur. Phys. J.: Appl. Phys. **43**, 357 (2008).
[27] G. W. Simmons and D. J. Dwyer, Surf. Sci. **48**, 373 (1975).
[28] C. F. Brucker and T. N. Rhodin, Surf. Sci. **57**, 523 (1976).
[29] K. O. Legg, F. Jona, D. W. Jepsen, and P. M. Marcus, Phys. Rev. B **16**, 5271 (1977).
[30] C. R. Brundle, Surf. Sci. **66**, 581 (1977).
[31] Y. Sakisaka, T. Miyano, and M. Onchi, Phys. Rev. B **30**, 6849 (1984).
[32] R. L. Headrick, P. Konarski, S. M. Yalisove, and W. R. Graham, Phys. Rev. B **39**, 5713 (1989).
[33] S. J. Roosendaal, B. van Asselen, J. W. Elsenaar, A. M. Vredenberg, and F. H. P. M. Habraken, Surf. Sci. **442**, 329 (1999).
[34] J.-P. Lu, M. R. Albert, S. L. Bernasek, and D. J. Dwyer, Surf. Sci. **215**, 348 (1989).
[35] V. Stambouli, C. Palacio, H. J. Mathieu, and D. Landolt, Appl. Surf. Sci. **70-71**, 240 (1993).
[36] F. Bisio, R. Moroni, M. Canepa, L. Mattera, R. Bertacco, and F. Ciccacci, Phys. Rev. Lett. **83**, 4868 (1999).
[37] P. Turban, L. Hennet, and S. Andrieu, Surf. Sci. **446**, 241 (2000).
[38] P. Muller, P. Turban, L. Lapena, and S. Andrieu, Surf. Sci. **488**, 52 (2001).
[39] P. Sautet, Surf. Sci. **374**, 406 (1997).
[40] M. O. Pedersen, L. Osterlund, J. J. Mortensen, M. Mavrikakis, L. B. Hansen, I. Stensgaard, E. Laegsgaard, J. K. Norskov, and F. Besenbacher, Phys. Rev. Lett. **84**, 4898 (2000).
[41] K. von Bergmann, M. Bode, A. Kubetzka, M. Heide, S. Blugel, and R. Wiesendanger, Phys. Rev. Lett. **92**, 046801 (2004).
[42] A. Cattoni, D. Petti, M. Cantoni, R. Bertacco, and F. Ciccacci (unpublished).
[43] C. Heiliger, P. Zahn, B. Y. Yavorsky, and I. Mertig, Phys. Rev. B **77**, 224407 (2008).